Available online at www.sciencedirect.com
ScienceDirect
Journal of the European Ceramic Society 30 (2010) 2131–2138
www.elsevier.com/locate/jeurceramsoc

Effect of WC or NbC addition on lattice parameter of surrounding structure in $Ti(C_{0.7}N_{0.3})$–Ni cermets investigated by TEM/CBED

Seongwon Kim [a,b,c,*], Jian-Min Zuo [b], Shinhoo Kang [c]

[a] *Engineering Ceramic Center, Korea Institute of Ceramic Engineering and Technology,30 Gyeongchung Rd., Icheon, Gyeonggi-do 467-843, Republic of Korea*
[b] *Department of Materials Science and Engineering, University of Illinois at Urbana-Champaign, IL 61801, USA*
[c] *Department of Materials Science and Engineering, Seoul National University, Seoul 151-744, Republic of Korea*

Received 10 July 2009; received in revised form 22 February 2010; accepted 17 March 2010
Available online 4 May 2010

Abstract

The changes in the lattice parameters of the solid solutions in the $Ti(C_{0.7}N_{0.3})$–WC–Ni and $Ti(C_{0.7}N_{0.3})$–NbC–Ni systems were first shown quantitatively by the CBED (Convergent Beam Electron Diffraction) technique together with TEM (Transmission Electron Microscopy) microstructure characterization. The extent of the changes in the lattice parameters between core and rim differs in the case of WC and NbC additions. No change in the lattice parameters is observed in the $Ti(C_{0.7}N_{0.3})$–WC–Ni cermets, in contrast to the Ti(C,N)–NbC–Ni cermets where significant changes in the lattice parameters are observed. The difference in the parameters is correlated with the core/rim structure, which disappears in the Ti(C,N)–NbC–Ni cermets when a large amount of NbC is added, and is discussed based on thermodynamic arguments. Large strain in the core and rim structure, especially near the core/rim interface, is also observed from the HOLZ (High Order Laue Zone) line splitting.

Keywords: Cermets; Core/rim structure; Lattice parameter; CBED (Convergent Beam Electron Diffraction)

1. Introduction

Ti(C,N)-based cermets are dense, hard materials which are important components in high-speed cutting tools.[1,2] Compared to the cutting performance of the conventional tool materials made of WC–Co, Ti(C,N)-based cermets provide improved surface finishing, excellent chip and tolerance control, and good geometrical accuracy of the work-pieces.[3] These characteristics are attributed to the mechanical properties of the hard phases, which are retained in the cermets. The typical microstructure of the hard phase in the cermets is the core/rim structure. Core/rim structures consist of undissolved Ti(C,N) cores and surrounding rim phases of (Ti,W,Nb,. . .)(C,N) solid solutions. Rim structures are also stated as surrounding structures. It is generally accepted that dissolution–reprecipitation,[4] rather than spinodal decomposition[5] or diffusion,[6] is the main mechanism involved in the formation of the core/rim structure.

The major ingredients of the hard phases are transition metal (Group IV) carbides and nitrides which have B1 structure (NaCl structure) with different lattice parameters.[7,8] In the Ti(C,N)-based cermets, the carbides and nitrides dissolve into the liquid binder and precipitate to form a solid solution in the form of a rim structure during liquid-phase sintering. One of the major interests in these cermets is to develop an understanding of the formation process of the core/rim structure when various carbides and nitrides are, individually or multiply, added to the Ti(CN)-based system. In such cases, the cores are undissolved Ti(C,N) particles and the rim phases are made up of newly formed carbonitride solid solutions such as (Ti,W,Nb,. . .)(C,N). A previous report showed that the rim phases present in the final microstructure form and grow mainly during liquid-phase sintering.[4] The compositions and lattice parameters of the rim structures have also been characterized using EDS (Energy Dispersive Spectrometry)[9–11] and XRD (X-ray Diffraction),[12,13] respectively. However, XRD does not have the spatial resolution required to map the lattice parameters in the core/rim structure.

Herein, we report a TEM study of the core/rim structure in Ti(C,N)-based cermets with compositions close to those of the commercial cermets. In the first part of this study, the effect of WC or NbC additions on the microstructures of the

* Corresponding author at: Engineering Ceramic Center, Korea Institute of Ceramic Engineering and Technology, 30 Gyeongchung Rd., Icheon, Gyeonggi-do 467-843, Republic of Korea. Tel.: +82 31 645 1452; fax: +82 31 645 1485.
E-mail address: woods3@kicet.re.kr (S. Kim).

0955-2219/$ – see front matter © 2010 Elsevier Ltd. All rights reserved.
doi:10.1016/j.jeurceramsoc.2010.03.006

$Ti(C_{0.7}N_{0.3})$–Ni system is investigated using Z-contrast STEM (Scanning Transmission Electron Microscopy) and compared with previously reported studies of the $Ti(C_{0.7}N_{0.3})$–WC–Ni and $Ti(C_{0.7}N_{0.3})$–NbC–Ni systems.[11,12,14] In the second part of this study, the lattice parameters and composition of the rim structure are examined using the CBED, and EDS techniques. The relationship between the change in the lattice parameters and the microstructural evolution of the core/rim structure is discussed in terms of thermodynamic considerations.

2. Experimental procedures

$Ti(C_{0.7}N_{0.3})$–xWC–20Ni (in wt.%, $x = 5$, 15, 25) and $Ti(C_{0.7}N_{0.3})$–yNbC–20Ni (in wt.%, $y = 10$, 15, 20) cermets were prepared for this study using $Ti(C_{0.7}N_{0.3})$ (1–3 μm, Kennametal Inc.), WC (~2 μm, H.C. Starck), NbC (~1 μm, H.C. Starck) and Ni (3–4 μm, Novamet) powders. The samples were prepared by the conventional powder metallurgy technique. After weighing them, the powders were mixed by attrition milling with WC–Co balls in acetone for 10 h. The dried powder mixtures were then compacted into a disc form under a uniaxial pressure of 100 MPa. The discs were sintered at 1450 °C for the $Ti(C_{0.7}N_{0.3})$–xWC–20Ni system and at 1510 °C for the $Ti(C_{0.7}N_{0.3})$–yNbC–20Ni system. The sintering was carried out for 1 h in a vacuum furnace.

For the TEM analysis, the slices of the materials were cut into small pieces and polished on one side by a tripod polisher with an L-bracket attachment down to a thickness of 100 μm using diamond lapping films. The specimen polished on one side was then attached to copper TEM grids using M1 bond and polished on the other side to produce a wedged shape,[15] in order to minimize the ion-milling time. The thinned wedge was then ion-milled using 5 kV Ar ions with the incident angle of 15–8°. Thin foils of the cermets were examined by a TEM (JEOL JEM 2010F STEM, Japan) equipped with a GIF (Gatan Imaging Filter) and EDS analyzer.

The CBED patterns were recorded in STEM mode. The sample was first observed using a HAADF (High Angle Annular Dark Filed) detector, which has the inner cutoff angle of ~70 mrad. A small electron probe was then positioned in the region of interest using the STEM scanning coils and the energy-filtered CBED pattern was recorded using a GIF and CCD (Charge-coupled Device) camera placed after the GIF. The energy dispersive X-ray spectrum from the same region of interest was obtained simultaneously. Energy filtering was carried out using an energy slit with a width of 8 eV centered around the zero-loss peak to enhance the contrast of the recorded CBED patterns.

3. Results

3.1. Effect of WC or NbC on the microstructure of $Ti(C_{0.7}N_{0.3})$–20Ni

It has been previously reported that the addition of WC or NbC has different effects on the microstructure of the $Ti(C_{0.7}N_{0.3})$–20Ni system.[11,14] In our previous study of $Ti(C_{0.7}N_{0.3})$–WC–Ni systems,[11] the $Ti(C_{0.7}N_{0.3})$–5–25WC–20Ni system exhibited a typical core/rim structure independent to the WC content. The rim structure consists of two different regions, which are commonly referred to as the inner and outer rims. The inner rim is a carbonitride solid solution located adjacent to the Ti(C,N) cores and is usually rich in heavy elements. A representative microstructure is shown in Fig. 1(A). This image was taken by the HAADF detector in STEM mode and the contrast is related to the elemental weights. The inner rim appears light gray in these micrographs, whereas the outer rim rich in Ti is dark gray.

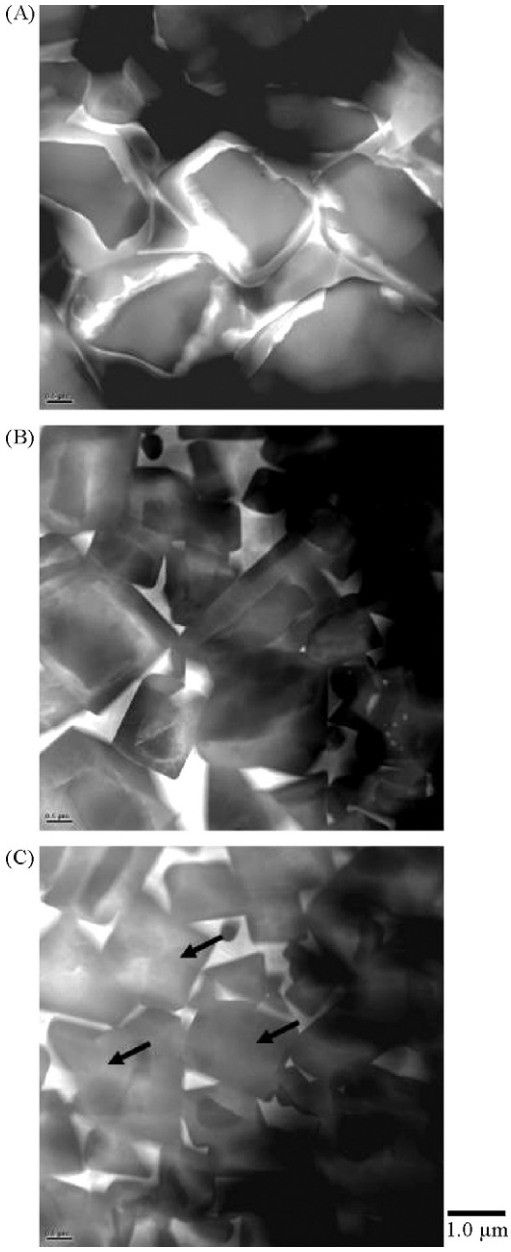

Fig. 1. HAADF (High Angle Annular Dark Field) images of $Ti(C_{0.7}N_{0.3})$–xMC–20Ni (in wt.%) sintered at 1450 °C for 1 h under a vacuum: (A) 15WC, (B) 10NbC, and (C) 20NbC (the arrows indicate solid solution grains without cores).

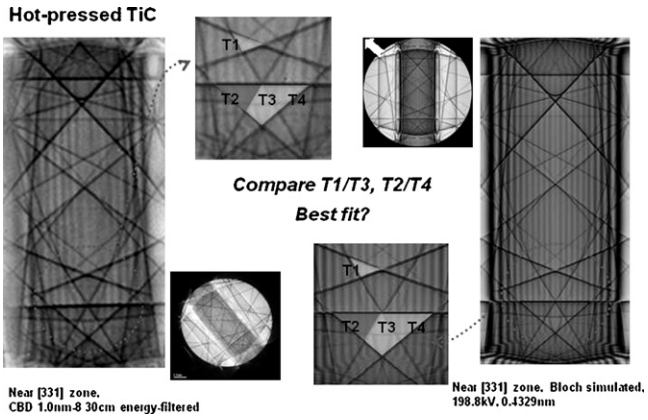

Fig. 2. A schematic illustration showing the technique used for measuring the lattice parameter from the recorded CBED pattern.

In the case of NbC addition, the evolution of the $Ti(C_{0.7}N_{0.3})$–Ni microstructure is different from that observed in the case of WC addition. This difference becomes obvious as the NbC content increases. Fig. 1(B) and (C) shows the microstructures of $Ti(C_{0.7}N_{0.3})$–Ni system which contains 10 and 20 wt.% NbC, respectively. The microstructure with a low level of NbC (<10 wt.%, Fig. 1(B)) shows a typical core/rim structure with somewhat faceted grains, as compared to the microstructure of the $Ti(C_{0.7}N_{0.3})$–WC–Ni system. Further increasing the NbC content, however, resulted in the appearance of solid solution grains without Ti(C,N) cores (arrows in Fig. 1(C)). The modification of core/rim structure to solid solution grain without Ti(C,N) core is the peculiar microstructure observed in Ti(C,N)–NbC–Ni system.[12,14] In contrast to the previous works,[12,14] the appearance of Ti(C,N) particles without rims is not obvious in the present study. Since the particle size of the commercial grade Ti(C,N) powder used in this study is smaller, the Ti(C,N) particles are dissolved fast during the sintering process.

The driving force for the reactions in most materials systems is the reduction in the total free energy of the systems.[16] The three dominating energies involved in the liquid-phase sintering of solid solution cermets are (1) the free energy of mixing, (2) the strain energy due to compositional gradients and/or lattice mismatch and (3) the interfacial energy at the solid–liquid interfaces.[17–19] Among these energy terms, the contribution of the strain energy becomes important in the core/rim structure.

3.2. Measurement of the lattice parameter using CBED

Fig. 2 shows the procedure used to measure the lattice parameters with CBED in this work.[20] When a convergent beam is used for diffraction, the diffracted beams appear as disks instead of sharp spots, as in conventional SAED (Selected Area Electron Diffraction), because of the beam convergence. The accuracy of SAED for the measurement of the lattice parameters is limited to an error of about 0.1–1% depending on the instrumental setup. The accuracy is significantly improved by using the HOLZ lines observed in CBED.[21,22] The positions of the HOLZ lines are sensitive to the local lattice parameters under the electron beam and the electron wavelength. Furthermore, the area of analysis, which is several nanometers in diameter, is defined clearly by the focused electron beam. This spatial resolution is useful in the analysis of fine microstructural features such as core/rim structures.

The lattice parameters are measured from the recorded CBED pattern by comparing the simulated CBED patterns with the experimental ones, in order to find the best fit. In general, better accuracy is obtained by including the dynamic effects in the simulation and employing the Bloch wave method,[23] which was used in this study. For the study of the lattice parameters, the high tension of the microscope was calibrated using a Si crystal. The calibrated high tension of the JEM 2010F used in this work was 198.8 kV. The error range in the measurement of the lattice parameters is within 0.1%. The energy-filtering used herein enhances the contrast of the high order HOLZ lines, which are more sensitive to the changes in the lattice parameters. The changes in the lattice parameters in the core and rim structure in the Ti(C,N)–WC–Ni or Ti(C,N)–NbC–Ni cermets were measured using the CBED patterns recorded near the [3 3 1] zone axis orientation. The compositions of the cores and rims, in the region where the CBED patterns were taken, were also analyzed simultaneously by EDS. The results are shown in Figs. 3–6. The measured lattice parameters are shown below along with the simulated, best-fit CBED patterns. The compositions of the heavy atoms in the rim structures were converted into elemental ratios.

4. Discussion

4.1. Effect of secondary carbides on the lattice parameter

4.1.1. WC effect

Among the different compositions studied herein, the lattice parameters of all the cores are approximately the same, regardless of the amount of WC or NbC added (Fig. 3). The measured lattice parameters of the core are 0.4302 nm. The lattice parameters of TiC and TiN are known to be 0.4327 and 0.4241 nm, respectively (*JCPDS 1987 and 1981*). Thus, assuming that the cores are undissolved Ti(CN), the calculated composition of the cores is $Ti(C_{0.71}N_{0.29})$ based on Vegard's law for solid solution phases assuming that Ti(C,N) is an ideal solid solution.[24] This is close to the original composition of the $Ti(C_{0.7}N_{0.3})$ phase and implies that the cores retain their initial composition. The results of the EDS measurements also agree with this conclusion.

Fig. 4 shows the HOLZ line splitting in the inner rim region, as indicated by arrows. We observed the HOLZ line splitting in some of recorded diffraction patterns for the inner rim. HOLZ line splitting is commonly observed in the CBED patterns recorded in samples with a large strain and strain relaxation.[25] Thus, these patterns with split HOLZ lines provide evidence of the existence of a large amount of strain in the inner rim region. Depending on the thickness and location of the rim, the strain exerted on the inner rim varies throughout the rim thickness in a complicated manner. The highest strain is to be expected at the core/inner rim interface, even if there exist misfit dislocations, which can behave as the most possible location of cracking during performance testing.

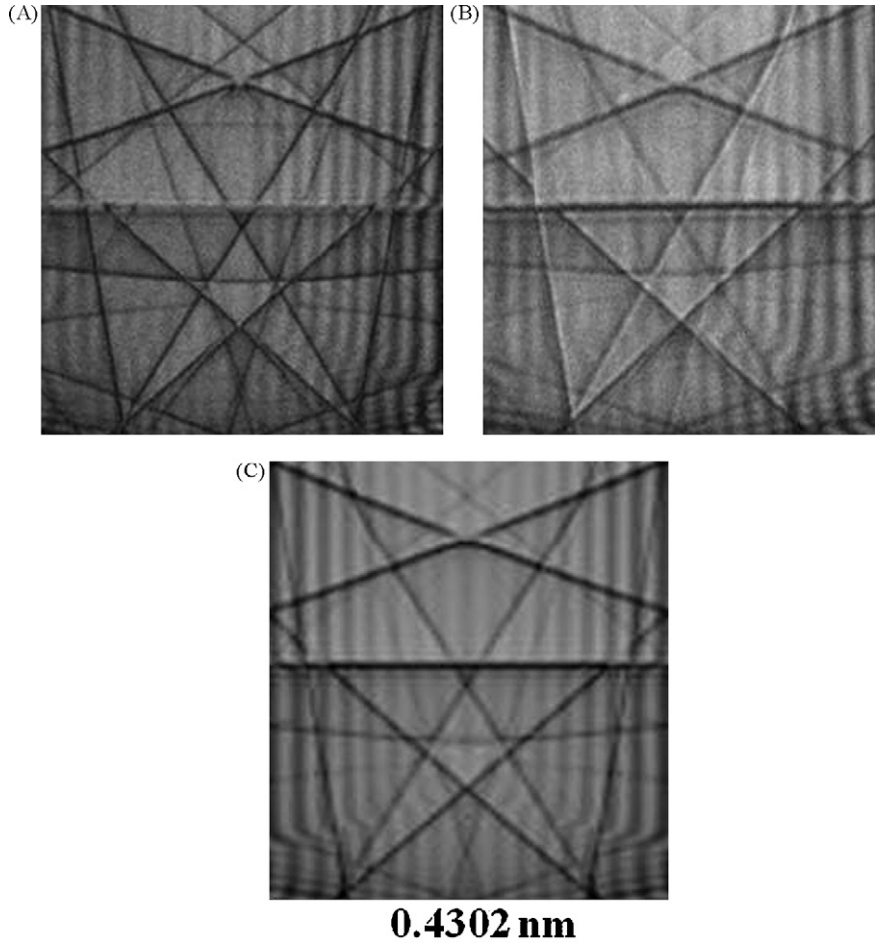

Fig. 3. Central parts of energy-filtered CBED patterns along the [3 3 1] zone axis from different cores of $Ti(C_{0.7}N_{0.3})$–*x*MC–20Ni (in wt.%) sintered at 1450°C for 1 h under a vacuum: (A) 5WC, (B) 20NbC, and (C) a simulated dynamical CBED pattern.

Fig. 5 shows the results of the CBED and EDS analyses, along with the measured lattice parameters of the outer rims in the Ti(C,N)–WC–Ni cermets. The lattice parameters of the rims are approximately the same as those of the cores even for different tungsten contents (from 5 to 25 wt.% of WC addition). Laoui et al.[26] reported that the CBED patterns from the core and rim in cermets were identical, which is consistent with our results in the case of WC addition.

In forming various solid solutions, the lattice parameter of a Ti(C,N) solid solution tends to decrease with increasing nitrogen content[7] and the same is true with regard to the tungsten content in (W, Ti)C or (Ti,W)C.[13] Thus far, few studies have been reported on the role of the elements in the determination of the (Ti,W)(C,N) lattice parameters. Tungsten in the (Ti,W)(C,N) solid solution is known to have poor affinity with nitrogen.[27] It was also reported that this poor affinity even results in nitrogen diffusion from the tungsten-rich rim to the titanium-rich core.[28] Such diffusion is less likely to happen between the inner and outer rims, since the inner rim has more W. Thus, the interaction between W and N in the phase will determine the lattice parameter. In order to explain the similar lattice constants of the various (Ti,W)(C,N) rim compositions, the nitrogen content decreases with increasing tungsten content, which is in line with the chemical stability issue.

The nitrogen that dissolves in the Ni melt at 1500 °C can either be changed into N_2 gas, which evaporates from the system during vacuum sintering, or remain in the melt to form a solid solution phase. The reaction to form N_2 is less likely, except near the surface regions, even though the solubility of nitrogen in the Ni melt is extremely small (<0.025 at.%). This is because the thermodynamic driving force for the formation of a solid solution is much higher than that of this reaction. Still, both reactions occur and the final nitrogen contents in the rim phases are less than the original content. As a result, the high W content did not seem to affect the lattice parameter and, consequently, the structure stabilizes at the initial lattice constant. Therefore, the outer rim phase retains the same lattice parameter, regardless of the rim composition.

It is interesting to compare the effect of the rim composition on the lattice parameter. In the case of the inner rim, the HOLZ line splitting is dominant, regardless of the composition. The inner rim that exists between the core and outer rim, which has the same lattice parameter, must be strained due to lattice mismatch. If the relationship between W and N in (Ti,W)(C,N) remains the same for both the inner and outer rims, no HOLZ line splitting would be observed. In general, the inner rim has a higher W content than the outer rim. However, the fact that the lattice parameter of the inner rim is the same as that of the

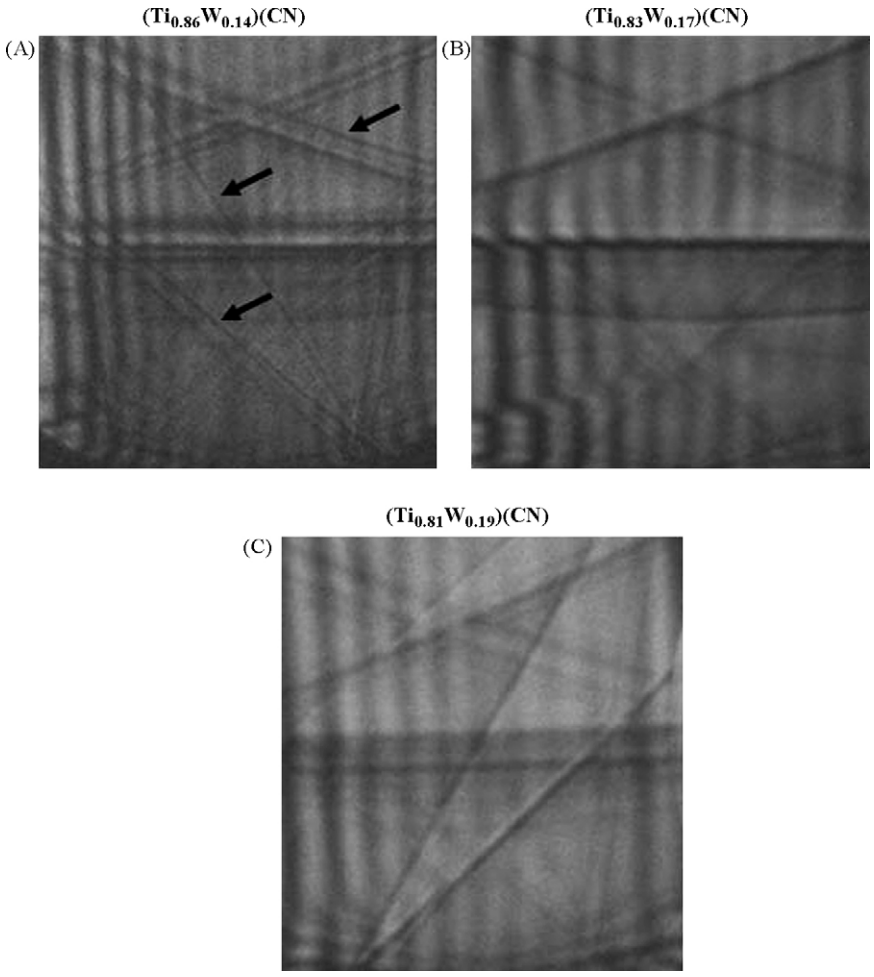

Fig. 4. Central parts of energy-filtered CBED patterns along the [3 3 1] zone axis from the inner rim of $Ti(C_{0.7}N_{0.3})$–xWC–20Ni (in wt.%) sintered at 1450 °C for 1 h under a vacuum: (A) $x = 5$, (B) $x = 15$, and (C) $x = 25$ (the compositions above the CBED patterns were obtained by EDS).

core does not necessarily mean that the inner rim contains less nitrogen than the outer rim. Rather, it tends to contain much more nitrogen than the outer rim, due to the availability of nitrogen when it forms during sintering. It would be expected for the inner rim to have a smaller lattice parameter than 0.4302 nm. These interfaces may become crack initiation sites during tool performance.

4.1.2. NbC effect

The change in the lattice parameters of the rims differs depending on the amount of secondary carbide added. The increase in the lattice parameter of the rims with the addition of NbC to Ti(C,N)–Ni cermets is notable compared to that observed with the addition of WC, as shown in Fig. 6. This is due to the larger atomic radius of Nb (0.143 nm) than that of W (0.137 nm) in the structure. Further, Nb also has less affinity with N and C than Ti. This is obvious when comparing the lattice parameter of Ti(C,N), 0.4302 nm, with that of $(Ti_{0.92}Nb_{0.08})$(C,N), 0.4323 nm. Nevertheless, Nb is known to have better affinity with N than W, which can be proven by measuring the free energy of nitride formation in each case.[7,27] The effects of Nb and W on the change in the ratio of C to N in the Ti(C,N) structure, B1, have yet to be defined.

The high spatial resolution of CBED allows the differentiation of the lattice parameters of the rim and core. The increase in the lattice parameter of the rims with the addition of NbC results in its being far beyond the range of the lattice parameter of Ti(C,N), 0.4302 nm. This provides a clue to the appearance of the (Ti,Nb)(C,N) solid solution without a core. In Fig. 1(A) the core/rim structure is maintained, regardless of the amount of WC in the $Ti(C_{0.7}N_{0.3})$–xWC–20Ni system. On the other hand, the structure, in the $Ti(C_{0.7}N_{0.3})$–NbC–Ni system, is changed into a coreless solid solution of (Ti,Nb)(C,N) when the NbC content exceeds 15 wt.% (Fig. 1(C)), which is consistent with our previous work.[12]

From the EDS results, it was found that the central parts of the solid solutions are not pure NbC. Instead, the compositions of these phases are closely matched to those of the rim of the particles. This strongly suggests that this phase is formed as the rim phase, as stated in our previous work.[12] The phase that is supposed to form as the inner rim, if allowed, is homogeneously nucleated and grows in the Ni melt. The precipitates of the rim phase in the melt also become heterogeneous sites for the nucleation of the phase formed later. Fig. 1(C) shows the result of this precipitation.

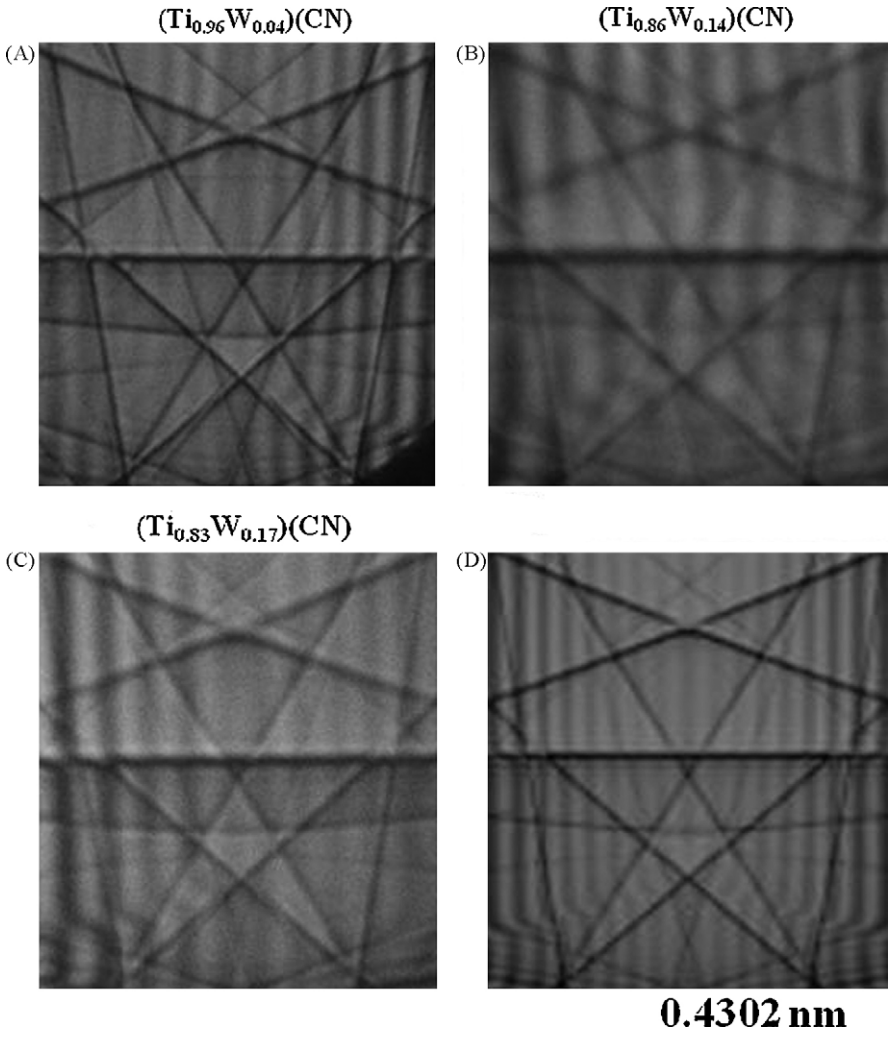

Fig. 5. Central parts of the energy-filtered CBED patterns along the [3 3 1] zone axis from the outer rim of $Ti(C_{0.7}N_{0.3})$–xWC–20Ni (in wt.%) sintered at 1450 °C for 1 h under a vacuum: (A) $x = 5$, (B) $x = 15$, and (C) $x = 25$, and (D) a simulated dynamical CBED pattern. The compositions were obtained by EDS.

The lattice parameters were measured along with the compositions by EDS. The compositions of the newly formed phase in Fig. 6 were found to correspond to those of the outer rim phase.[12] Thus, the relevant lattice parameters of the inner rims were estimated by extrapolating the relationship between the Nb content in (Ti,Nb)(C,N) and the lattice parameter using the data in Fig. 6 and obtained from previous studies.[12,29] This relationship and the calculated lattice parameters are shown in Table 1.

If the lattice parameters of the unconstrained precipitate and matrix are a_β and a_α respectively, the unconstrained misfit δ is defined by

$$\delta = \frac{a_\beta - a_\alpha}{a_\alpha}$$

In the case of a coherent spherical particle, the distortion is purely hydrostatic, resulting in a new lattice parameter, a'_β. Then, the

Table 1
Lattice parameters and strain level in Ti(C,N)–xNbC–Ni core/rim structure.

Alloy[a]	Outer rim[28]		Inner rim[12]		Level of strain (mm/mm)	
	Composition via TEM/EDS	HOLZ analysis (nm)	Composition via TEM/EDS	Lattice parameter by extrapolation (nm)	δ at interface between core and inner rim	δ between inner and outer rims
Ti(C,N)–10NbC	$(Ti_{0.92}Nb_{0.08})(C,N)$	0.4323	$(Ti_{0.83}Nb_{0.17})(C,N)$	0.4338	0.0084	0.0035
Ti(C,N)–15NbC	$(Ti_{0.89}Nb_{0.11})(C,N)$	0.4323	$(Ti_{0.71}Nb_{0.29})(C,N)$	0.4361	0.0138	0.0067
	$(Ti_{0.87}Nb_{0.13})(C,N)$	0.4332				
Ti(C,N)–20NbC	$(Ti_{0.83}Nb_{0.17})(C,N)$	0.4336	$(Ti_{0.71}Nb_{0.29})(C,N)$	0.4361	0.0138	0.004
	$(Ti_{0.81}Nb_{0.19})(C,N)$	0.4344				

[a] The lattice parameter of Ti(C,N) core in the alloys above is 0.4302 nm.

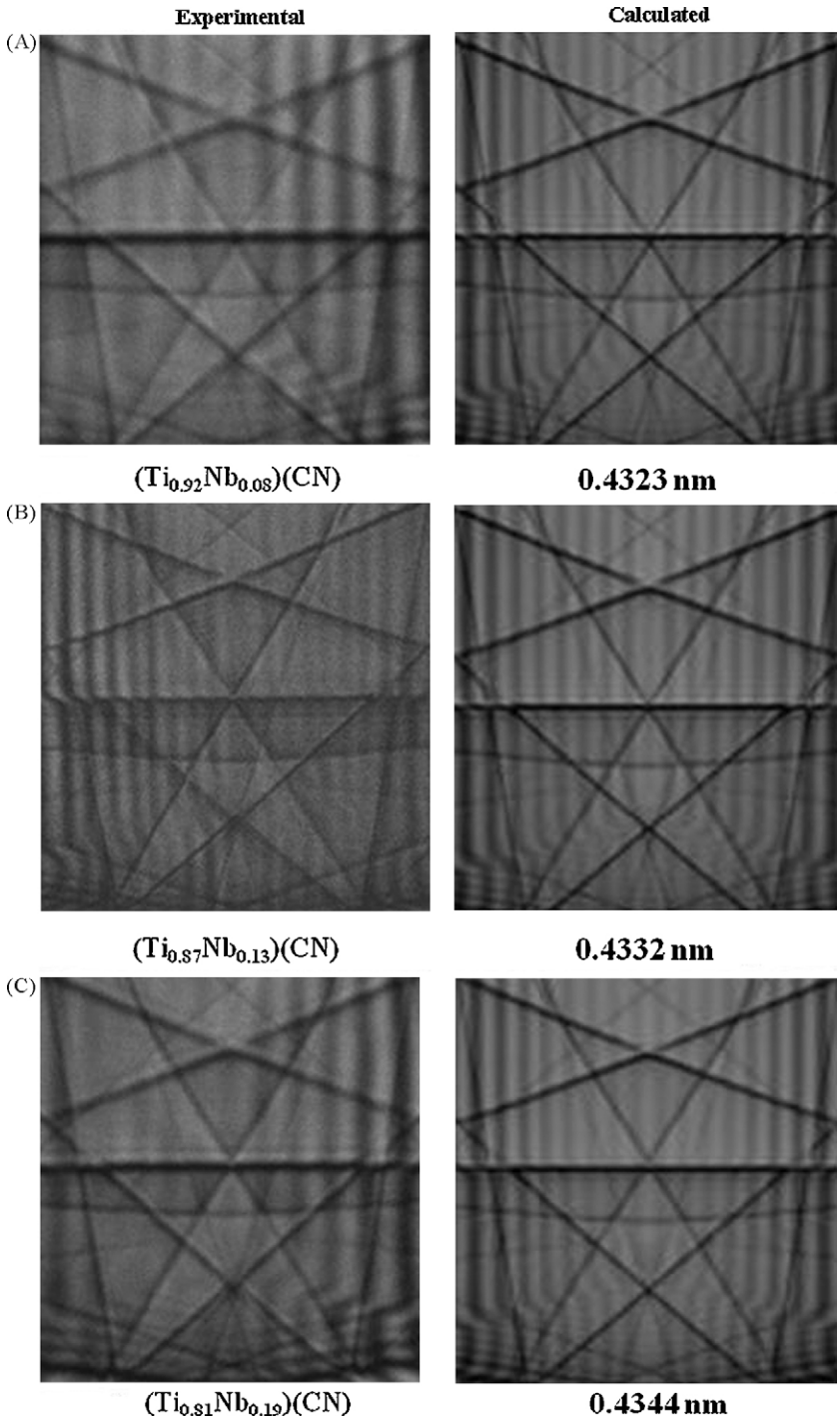

Fig. 6. Central parts of experimental energy-filtered and simulated dynamical CBED patterns along the [3 3 1] zone axis from the outer rims of $Ti(C_{0.7}N_{0.3})$–xNbC–20Ni (in wt.%) sintered at 1510 °C for 1 h under a vacuum: (A) $x = 10$, (B) $x = 15$, and (C) $x = 20$. The compositions above the CBED patterns were obtained by EDS.

constrained misfit ε is defined by

$$\varepsilon = \frac{a'_{\beta} - a_{\alpha}}{a_{\alpha}}$$

If the elastic moduli of the precipitate and matrix are the same and Poisson's ratio is 1/3, ε and δ are simply related by[30]

$$\varepsilon = \frac{2}{3}\delta$$

Since the thickness of the inner rim is normally small compared to that of the Ti(CN) core, the above relation holds. Based on the compositions of the inner rim, the unconstrained and constrained misfits were calculated and are listed in Table 1. From this study, the unconstrained misfit, δ, of the Ti(C,N)–>15NbC–Ni system turns out to be 1.38%, while the constrained misfit, ε, is 0.92%. The calculated misfits, δ and ε, between the inner and outer rims remain less than 0.67 and 0.45%, respectively. The XRD

prediction in Ref. 12 agrees well with this result. If we take this level of strain as a guideline for the phase separation, the lattice parameter of the inner rim be greater than 0.4243 nm for the Ti(CN)–xWC–Ni system of Fig. 4.

5. Conclusions

A comparative study of the microstructure and lattice parameters of the Ti($C_{0.7}N_{0.3}$)–WC–Ni and Ti($C_{0.7}N_{0.3}$)–NbC–Ni systems was carried out using CBED combined with the Transmission Electron Microscopy characterization of the microstructure. The results of the lattice parameter measurements of the two systems show that:

(1) In the Ti(C,N)–WC–Ni systems, the lattice parameters remained constant in both the core and rim structures.
(2) An increase in the lattice parameter is observed when NbC is added to the Ti(C,N)–Ni cermets. This suggests that the appearance of the (Ti,Nb)(C,N) solid solution without a core is caused by the high lattice mismatch at the core/inner rim interface.
(3) The critical unconstrained misfit, δ, which causes the separation of the inner rim in the Ti(C,N)–MC–Ni (M: W or Nb) systems, is in the vicinity of 1.38%. The presence of a large amount of strain was evidenced by the HOLZ line splitting in the core and rim structures, especially near the core/rim interfaces of both systems.

Acknowledgments

This work was supported by a grant-in-aid from the National Core Research Center Program of MOST and KOSEF (No. R15-2006-022-R15-2006-022-03001-0). The microscopy characterization was supported by DOE DEFG02-01ER45923. The electron microscopy work was carried out in the Center for Microanalysis of Materials, University of Illinois, which is partially supported by the US Department of Energy under grant number DEFG02-91-ER45439. Special thanks go to Dr. S.Y. Ahn at Korloy, Inc., Korea, for his help in the preparation of the manuscript.

References

1. Zhang SY. Titanium carbonitride-based cermets-processes and properties. *Mater Sci Eng A* 1993;**163**:141.
2. Ettmayer P, Kolaska H, Lengauer W, Dreyer K. Ti(C,N) cermets-metallurgy and properties. *Int J Refract Met Hard Mater* 1995;**13**:343.
3. D'Errico GE, Bugliosi S, Guglielmi E. Tool-life reliability of cermet inserts in milling tests. *J Mater Process Technol* 1998;**77**:337.
4. Suzuki H, Hayashi K, Terada O. Mechanisms of surrounding structure formation in sintered TiC–Mo_2C–Ni alloys. *J Jpn Inst Met* 1981; **35**:245.
5. Rudy E. Constitution of ternary titanium–tungsten–carbon alloys. *J Less-Common Met* 1973;**33**:245.
6. Moskowitz D, Humenik Jr M. Cemented titanium carbide cutting tools. *Mod Dev Powder Metall* 1966;**3**:83.
7. Toth LE. *Transition metal carbides and nitrides*. New York and London: Academic Press; 1971 p. 6–7.
8. Lengauer W, Binder S, Aigner K, Ettmayer P, Guillou A, Debuigne J, et al. Solid state properties of group IVb carbonitrides. *J Alloys Compd* 1995;**217**:137.
9. Lindahl P, Gustafson P, Rolander U, Stals L, Andrén HO. Microstructure of model cermets with high Mo or W content. *Int J Refract Met Hard Mater* 1999;**17**:411.
10. Chen L, Lengauer W, Ettmayer P, Dreyer K, Daub HW, Kassel D. Fundamentals of liquid phase sintering for modern cermets and functionally graded cemented carbonitrides (FGCC). *Int J Refract Met Hard Mater* 2000;**18**:307.
11. Ahn SY, Kang S. Formation of core/rim structures in Ti(C,N)–WC–Ni cermets via a dissolution and precipitation process. *J Am Ceram Soc* 2000;**83**:1489.
12. Ahn SY, Kim SW, Kang S. Microstructure of Ti(C,N)–WC–NbC–Ni cermets. *J Am Ceram Soc* 2001;**84**:843.
13. Saidi A, Barati M. Production of (W,Ti)C reinforced Ni–Ti matrix composites. *J Mater Process Technol* 2002;**124**:166.
14. Qi F, Kang S. A study on microstructural changes in Ti(C,N)–NbC–Ni cermets. *Mater Sci Eng A* 1998;**251**:276.
15. Benedict J, Anderson R, Klepeis SJ. Recent developments in the use of the tripod polisher for TEM specimen preparation. In: Anderson R, Tracy B, Bravman J, editors. *Specimen preparation for transmission electron microscopy of materials III, Materials research society symposium proceedings, vol. 254*. Pittsburgh, PA: Materials Research Society; 1992. p. 121–41.
16. Ahn S-Y, Kang S. Effect of WC particle size on microstructure and rim composition in the Ti(C0.7N0.3)–WC–Ni system. *Scripta Mater* 2006;**55**:1015.
17. Rhee WH, Yoon DN. The instability of solid liquid interface in Mo–Ni alloy induced by diffusional coherency strain. *Acta Metall* 1987;**35**:1447.
18. Chae KW, Chun DI, Kim DY, Baik YJ, Eun KY. Microstructural evolution during the infiltration treatment of titanium carbide iron composite. *J Am Ceram Soc* 1990;**73**:1979.
19. Chun DI, Kim DY, Eun KY. Microstructural evolution during the sintering of TiC–Mo–Ni cermets. *J Am Ceram Soc* 1993;**76**:2049.
20. Rozeveld SJ, Howe JM. Determination of multiple lattice parameters from convergent-beam electron diffraction patterns. *Ultramicroscopy* 1993;**50**:41.
21. Zuo JM. Quantitative convergent beam electron diffraction. *Mater Trans JIM* 1998;**39**:938.
22. Kim M, Zuo JM, Park G-S. High-resolution strain measurement in shallow trench isolation structures using dynamic electron diffraction. *Appl Phys Lett* 2004;**84**:2181.
23. Zuo JM, Mabon JC. Web-based electron microscopy software: web-Emaps. *Microsc Microanal* 2004;**10**:1000.
24. Pastor H. Titanium-carbonitride-based hard alloys for cutting tools. *Mater Sci Eng A* 1988;**106**:401.
25. Clement L, Pantel R, Kwakman LFT, Rouviere JL. Strain measurements by convergent-beam electron diffraction: the importance of stress relaxation in lamella preparations. *Appl Phys Lett* 2004;**85**:651.
26. Laoui T, Zou H, Van der Biest O. Analytical electron microscopy of the core/rim structure in titanium carbonitride cermets. *Int J Refract Met Hard Mater* 1992;**11**:207.
27. Doi A, Nomura T, Tobioka M, Takahashi K, Hara A. Thermodynamic evaluation of equilibrium nitrogen pressure and WC separation in Ti–W–C–N system carbonitride. In: *Proceedings of the 11th international Plansee seminar '85*. 1985. p. 825–43.
28. Zackrisson J, Rolander U, Andrén HO. Development of cermet microstructures during sintering. *Metall Mater Trans A* 2001;**32**:85.
29. Kim S. Dissolution–reprecipitation related phenomena in cermet system. PhD Thesis. Seoul, Korea: Seoul National University; 2006.
30. Eshelby JD. The determination of the elastic field of an ellipsoidal inclusion and related problems. *Proc R Soc A* 1957;**241**:376.